VI International Conference on Textile Composites and Inflatable Structures
STRUCTURAL MEMBRANES 2013
K.-U.Bletzinger, B. Kröplin and E. Oñate (Eds)

FAILURE OF POLYETHYLENE THIN FILM MEMBRANE STRUCTURES

Dezso Hegyi*, Jun Li† AND Sergio Pellegrino†

*Department of of Mechanics, Materials and Structures
Budapest University of Technology and Economics
1111 Budapest, Muegyetem rkp. 3., Hungary
e-mail: dizso@szt.bme.hu, web page: http://www.szt.bme.hu/

† GALCIT
California Institute of Technology
1200 E. California Blvd. Pasadena, CA 91125, USA
e-mail: sergiop@caltech.edu, web page: http://pellegrino.caltech.edu/

Key words: StratoFilm, J-integral, Viscoelasticity, Free Volume Model

Abstract. The failure of balloons made of Linear Low Density PolyEthylene (LLDPE) is investigated. The chosen film is 38 μm thick StratoFilm 420, currently used for the NASA Super-Pressure balloons [1]. The visco-elastic behaviour of the film has been extensively studied and is already accounted for in the balloon design [2, 3, 5]. The next step in the development of accurate predictive tools for super-pressure balloons requires models that capture the transition from visco-elastic and visco-plastic behaviour to fracture.

It is shown that realistic estimates of failure of LLDPE membrane structures can be obtained from visco-elastic simulations based on the non-linear visco-elastic model of the balloon film proposed by Kwok [5], supplemented with a fracture resistance criterion derived from the experimentally-based J-integral.

1 INTRODUCTION

The use of Linear Low Density PolyEthylene (LLDPE) films in NASA superpressure balloons has motivated extensive studies of their viscoelastic behavior in the small and large strain regimes. However, their viscoplastic behavior and ultimate failure have remained relatively unexplored, making it difficult to quantify the failure margins of structures built from such films. Currently balloon designers are forced to the conservatism of point-based stress failure criteria. The objective of the present study is to gain insight into the viscoplastic tearing of LLDPE films and to develop quantitative models that in future will enable rational estimates of load margins against viscoplastic failure by tearing.

Essential background for the present study are the small-strain nonlinear models [2, 3] and the large strain viscoelastic models [4, 5] for LLDPE films. A stress limit based on a 2 % strain offset is currently used as failure criterion in LLDPE balloon design, but such an approach is over-conservative in the case of localized stress peaks rise around geometry or stress singularities. Point-wise failure criteria neglect the stress redistribution that occurs near a stress peak and thus can significantly underestimate the reserve strength of a structure. A global approach that allows the stresses to redistribute until macroscopic yielding or tearing of the film occur is required to estimate the full strength.

Failure of polymers is usually approached by means of time-dependent yield criteria expressed in terms of stress components or energy. The time-to-failure of the polymer is captured by these criteria [6, 7, 8]. But no specific study of the time-to-failure of LLDPE film has been carried out. Tielking [9] carried out a series of complex tests on wide rectangular, semi-biaxial samples to obtain the relationship between crack amplitude and the J-integral.

Recent advances in experimental techniques, particularly in 3D digital image correlation, as well as large-strain constitutive modeling of LLDPE thin films have made it possible to obtain the critical values of the J-integral from direct strain measurements on a wide range of sample geometries. With this approach it is possible to obtain the complete relationship between crack amplitude and the J-integral from a single test, and hence it is possible to study strain rate effects in a direct way. It is hoped that these advances, presented in the present paper, will open the way to making direct connections between time-to-failure and crack propagation in thin films.

2 FAILURE OF POLYMERS

Uncrosslinked polymers, which include LLDPE, are used mainly above the glass transition temperature (T_g), to avoid brittle behavior. Hence, under normal operating conditions they can show significant time dependent deformation and plasticity. Their failure behavior also depends on time and temperature. For example, a test sample may be well below the breaking load measured at room temperature in a short-duration test, but it may fail when loaded for a longer period of time. Also, at lower temperature its strength increases.

The prediction of failure for such materials has been modeled by defining a function (failure criterion) that relates stress, strain and several other time-dependent parameters to a time-dependent yield stress.

One approach [18, 19] considers the function:

$$f = \frac{1}{2}\sigma_{ij}\sigma_{ij} - \left(A + B\exp\left(-C\sqrt{(\epsilon_{ij}^V - \epsilon_{ij}^E)\cdot(\epsilon_{ij}^V - \epsilon_{ij}^E)}\right)\right)^2 = 0, \tag{1}$$

where σ_{ij} is the stress tensor, ϵ_{ij} is the strain tensor and the superscripts V and E denote viscous and elastic components. Note that Eq. 1 is defined in terms of a Mises equivalent

stress (first term) and a time-dependent yield stress (second term). A, B and C are material parameters.

Alternatively, it is assumed that failure is linked to the stored strain energy reaching a critical level, without accounting for viscous or plastically dissipated energy [20, 21, 22]. Furthermore, only the deviatoric component of the strain energy is considered, not the dilatational energy. Since, the time-dependent stress and strain components can be estimated from a finite element analysis, implementation of the latter approach requires only a single failure parameter to be defined and hence it is simpler to implement this approach than the three-parameter criterion in Eq. 1.

An alternative approach to the failure of polymer films relates failure to the propagation of a crack [9]. In fracture mechanics the J-integral is a useful tool to analyze problems involving crack propagation in inelastic materials. The J-integral is the integral of the energy release rate on a contour that surrounds the crack tip. It is path independent and in elastic fracture mechanics it is equal to the energy release rate, i.e. the fracture energy per unit surface of crack [23], Fig. 2. It can be calculated from:

$$J = \int_{\Gamma} \left(W n_1 - T \frac{\partial u}{\partial x} \right) \mathrm{d}s, \tag{2}$$

where Γ is the chosen contour, W is the strain energy, n_1 is the component of the normal strain in the direction normal to Γ, T is the stress normal to Γ, u is the movement of the crack tip, x is defined parallel to the crack and $\mathrm{d}s$ is an infinitesimal element along Γ.

When a critical level of the J-integral is reached the crack starts to propagate. The J-integral is usually plotted as a function of the crack length increase, Δa, Fig. 1. J_c is the critical value of J when the crack size starts to increase. The slope of the J-curve beyond J_c indicates the resistance of the material to crack propagation.

In elastic materials, plane-stress state, the toughness, K, is directly related to the energy release rate, G, and to J, by

$$\frac{K^2}{E} = G = J \tag{3}$$

In the case of inelastic materials there are difficulties in considering the toughness because some energy is dissipated, but the J-integral still gives a general method to determine the energy release associate with the crack propagation, and can be determined by using the stress-strain relation far from the crack-disturbed area.

Tielking [9] carried out unidirectional load tests on 76 mm long and 254 mm wide samples of 20 μm thick StratoFilm. Because of the large width to length ratio of these samples, the effect of their edge deformation on crack propagation is negligible. The J-integral could be evaluated indirectly from the equation [24]:

$$J = \frac{1}{B} \frac{\partial W_T}{\partial a}, \tag{4}$$

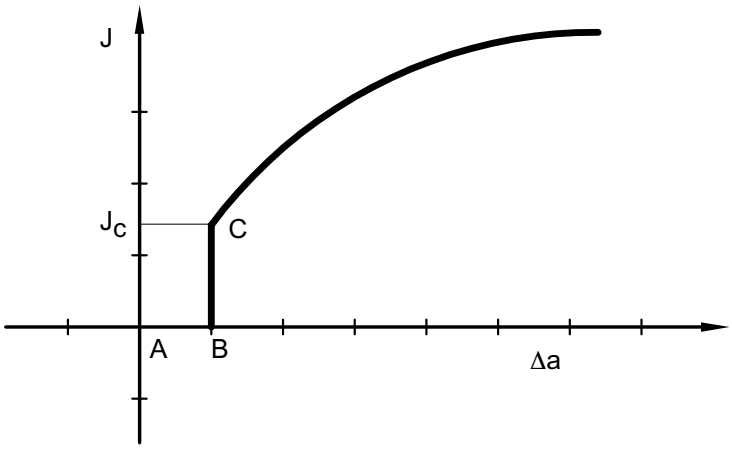

Figure 1: Schematic diagram of J-integral.

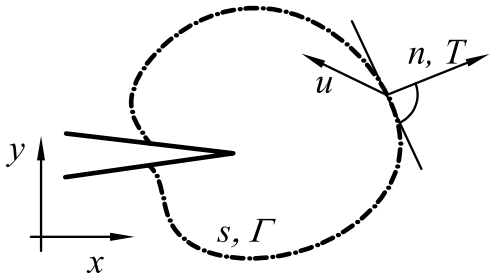

Figure 2: Integration path around the crack tip.

where B is the thickness of the sample, W_T is the total work of the loading mechanism and a is the half length of the crack. The J-integral can be determined by a multiple loading-unloading procedure using this equation; each point of the $J - \Delta a$ diagram can be determined from the difference between the loading-unloading energies and the change in Δa.

3 FAILURE BY VISCOELASTIC TEARING: PRELIMINARY TESTS

To obtain an initial understanding of the failure of StratoFilm 420 three sets of preliminary tests were carried out on 75 mm long and either 6 or 12 mm wide laser-cut dogbone samples, with the machine direction of the film aligned with the longer dimension of the sample. These tests investigated the difference in behavior between pristine film vs. film damaged by introducing a pinhole or a small slit.

The tests were carried out in an Instron 3119-506 environmental chamber at temperatures between 203 K and 263 K, using an Instron 5569 electromechanical materials testing machine. The ultimate strength, f_u, and ultimate extension, u_u, were determined from the peak in the load-extension diagram generated by the Instron BlueHill software. The full set of results is presented in Table 1. Note that in the case of samples that failed after extensive plastic deformation f_y and f_u refer to the original cross-section and hence do not reflect the true stress state in the necked sample. Representative snapshots from each set of tests are shown in Fig. 3(a-d) and the load-extension plots for four representative tests are presented in Fig. 3(e).

The first set of tests was carried out on samples that had no visible initial damage. Tests at two different strain rates, 1.33×10^{-3} s^{-1} and 2.66×10^{-3} s^{-1}, and two different temperatures, 263 K and 223 K, on 6 mm and 12 mm wide samples showed similarly large stretching (100-300 %) followed by the formation of a neck and failure of the sample. In all of these tests there was a significant amount of plastic deformation, as evidenced by the milky appearance of the sample (crazing). At the higher temperature (263 K) the full length of the inner part of the samples developed uniform crazing. At the lower temperature (223 K) the crazing started at one end of the sample (in the case shown in Fig. 3(b) crazing started at the bottom) and propagated through the full length of the sample before necking began. The ultimate stress was higher at the lower temperature and at the higher strain rate. This type of behavior is described with good accuracy by the energy-based failure criteria in Sec. 2, apart from the need to account for the large elongation before failure. The observed dependence of the ultimate stress on temperature is also well described by this approach.

The second set of tests was carried out on samples that had been initially damaged by introducing a pinhole in the middle. The idea for this test, which was done only at the lower temperature of 223 K, was that the pinhole might provide an initiation point for a crack that tears through the sample before a large amount of crazing occurs. However, extensive crazing was still observed before failure in this set of tests. Crazing always started at a point away from the pinhole, usually near one of the ends of the sample, and

Table 1: Results of preliminary failure tests. Width $[mm]$, Temperature [K], Humidity [%], Rate $[mm/s]$, yield stress (f_y) $[N/mm^2]$, breaking stress (f_u) $[N/mm^2]$, ultimate extension (u_u) $[mm]$.

	Test 1: no hole								Test 2: pinhole		Test 3: slit			
Width	12	**12**	6	**6**	12	**12**	6	**6**	12	**12**	12	**12**	12	**12**
Temp.	263	**263**	263	**263**	223	**223**	223	**223**	223	**223**	223	**223**	223	**203**
Hum.	75	**85**	85	**30**	40	**40**	35	**35**	40	**40**	40	**40**	20	**20**
Rate	0.1	**0.2**	0.1	**0.2**	0.1	**0.2**	0.1	**0.2**	0.1	**0.2**	0.1	**0.01**	0.001	**0.001**
f_y	16	**15**	14	**14**	24	**26**	15	**15**	26	**26**	22	**26**	26	**34**
f_u	17	**16**	24	**15**	26	**26**	17	**14**	22	**24**	22	**26**	26	**34**
u_u	190	**210**	210	**150**	100	**110**	60	**35**	60	**35**	3	**3**	3	**2.5**

propagated through the sample until it reached the pinhole. At this point the sample broke by propagation of a tear. The measured ultimate strength was in the same range as in the tests without pinhole but this time the ultimate extension of the sample was significantly smaller, see Fig. 3(e). Hence, it was concluded that a pinhole has no appreciable effect on the global strength of a sample but it does affect the maximum global deformation.

The third set of tests was carried out on 12 mm wide samples in which a central 2 mm transverse slit had been introduced. In this case crazing first appeared near the tips of the slit, which rapidly expanded and tore through the sample. The ultimate extension was much smaller than in the previous two cases, see curve (d) in Fig. 3(e), however, the ultimate strength values were in the same range as for the other types of samples.

The tests on initially undamaged samples showed a large amount of visco-plastic deformation. Lower temperatures caused the strength to increase, as expected from the failure criterion approach in Section 2. However, doubling the strain rate did not increase the strength as had been expected from the failure criterion. Introducing a pinhole or a slit in the sample did not change the overall strength but it substantially decreased the ultimate elongation.

These results were useful in planning further, more detailed experiments. Since all three sample configurations had provided approximately the same ultimate strength, the choice between pristine, damaged by a pinhole, or damaged by a slit was made on the basis of which configuration is most suited to producing the highest resolution in the strain field near the crack that ultimately tears through the sample. This strain field can be used to evaluate the J-integral around the crack. Here the key factor is the limited viewing field over which Digital Image Correlation systems can produce high-resolution strain fields. In order to image a narrow region of the sample, and to avoid that this region moves out of the viewing field during the test, the third sample configuration was selected.

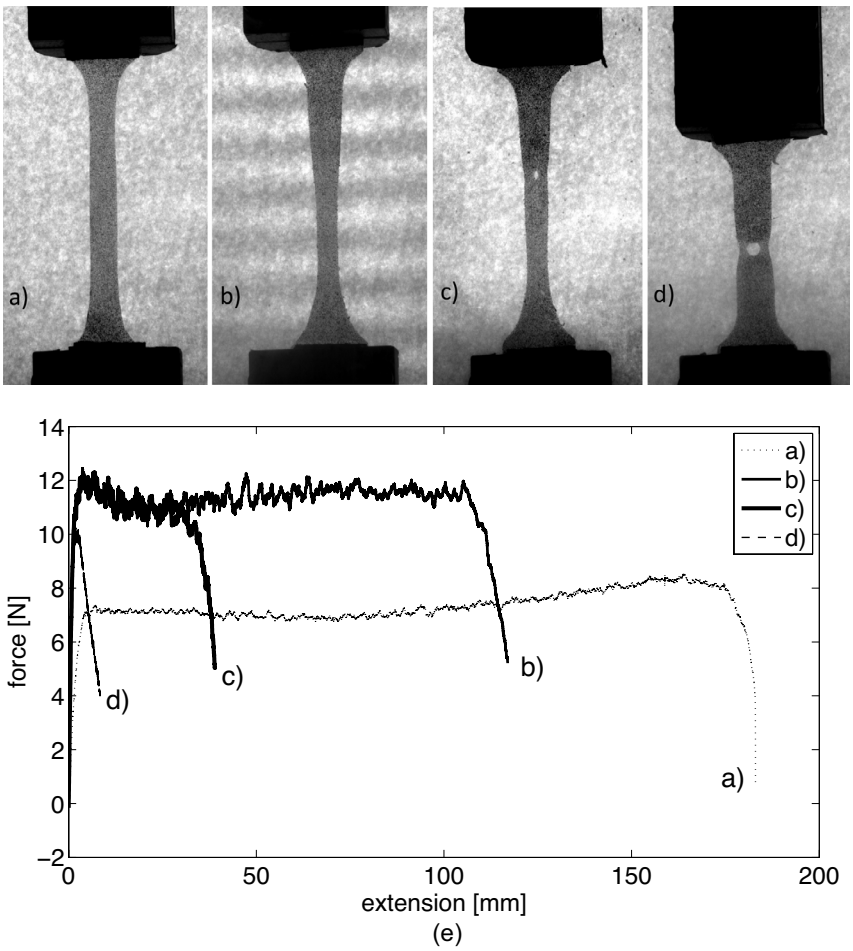

Figure 3: Snapshots from four tests: (a) no hole, T=263 K; (b) no hole, T=223 K, (c) pinhole, T=223 K; (d) slit (a=2 mm), T=223 K. (e) Force-extension diagrams for the four tests.

4 TEST APPARATUS AND SAMPLE CONFIGURATION

The strain in the film was measured with the Correlated Solutions Vic-3D 2010 Digital Image Correlation (DIC) system. The use of three-dimensional DIC allowed us to capture the effects of out of plane deformations, including wrinkling of the film. The test configuration can be seen in Figure 4; the cameras were Point Gray GRAS-50SSM-C with Pentax 75 mm F/2.8 lenses, set up with a field of view of approximately 50 mm. The test samples were lightly sprayed with black paint to provide a random speckle pattern with average size of 0.25 mm; they were captured at a rate of 1 s. The images were processed with Vic-3D using a correlation subset of 29×29 pixels and the strain field was computed from an 8-tap B-spline interpolation of the displacement field [25]. The crack length, $2a$, defined as the distance between the crack tips, was measured manually from the images. The pixel distance was measured and it was converted to the actual value using the initial 2 mm length of the slit as a calibration length.

Two types of tests were carried out: unidirectional tests on 12.7 mm (half inch, ASTM D-412 A) dogbone samples, and bidirectional tests on spherical bubbles obtained by inflating a circular sample with diameter of 125 mm, clamped around the edge. Both sets of samples contained a 2 mm wide slit in the middle, made with a scalpel. In the first test the machine direction of the film was aligned with the loading direction. The second test used an air pressure box with a 125 mm diameter hole, see Figure 5. StratoFilm samples were clamped over the box and the box was connected to an Omega IP610-030 pressure regulator. The applied pressure was measured with an Omega DPG409-015G electronic pressure gauge. The deformed shape of the test sample was measured with DIC and the strain field near the crack was obtained with Vic-3D using the same settings described above. Air leakage through the slit was prevented by means of an inner layer of wrap foil liner. According to a preliminary FEM analysis of the inflation of the film, the maximum stress occurs in the middle of the bubble and hence the slit for the crack analysis was placed there.

All tests were performed at 253 K, starting half an hour after closing the door of the environmental chamber and setting the controller at this temperature.

5 J-INTEGRAL DIAGRAMS

The J-integral defined in Eq. 2 requires the strain energy and the stress components to be known along the chosen contour Γ. Since the integral is path independent, it is best to choose Γ to be as far as possible from the crack tip, to keep the strains smaller and achieve greater accuracy in the stress calculation. Note that the integral should start from the edge of the crack, but standard DIC cannot measure strains close to a free edge.

The J-integral has been calculated along an approximately elliptical path with semi-axes of ~ 3 mm and ~ 4 mm, see Figure 6. The calculation has been repeated for each time step, using time-smoothed strain energy and stress values, and for each of the three tests that had been carried out.

Figure 4: Instron thermal chamber with DIC cameras.

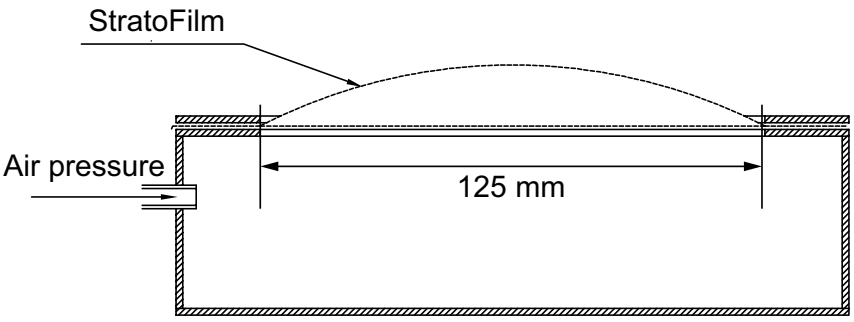

Figure 5: Section of pressure box for bidirectional tests.

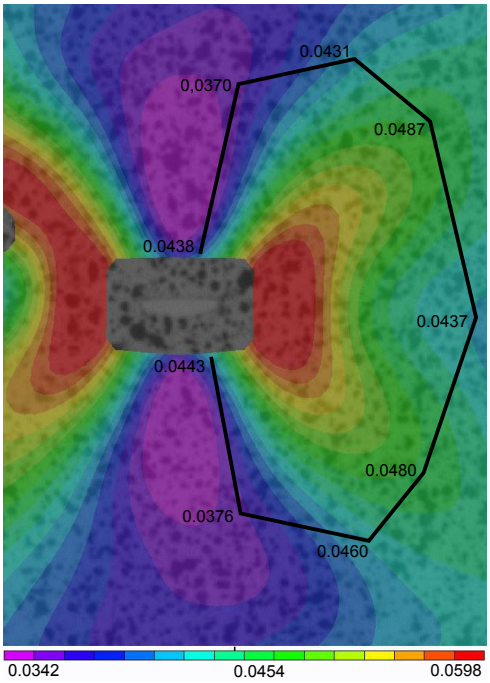

Figure 6: Strains around the crack tip. The rounded rectangle at the center has been excluded from the strain calculation.

The standard J-integral vs. crack propagation diagrams for the three tests are shown in Figs 7-9. Each figure shows the values of the J-integral around the left crack tip (A) and the right crack tip (B), and both the elastic strain energy and the total work are also plotted.

The results of the tests have been corrected to remove the effects of the transverse deformation of the sample, which causes an overall change in the crack length without any movement of the crack tip, Figure 10. The average transverse deformation was measured parallel to the crack, and the actual size of the crack was corrected with this deformation value.

Figures 7-9 show that the difference between elastic strain energy and the total work is small. This is not surprising because all of the tests were carried out at low temperature and they lasted no longer than half an hour.

The differences between the J-integrals for the A and B sides in the uniaxial tests, Figures 7-8, are larger than for the bubble test, Figures 9, because the loading arrangement for uniaxial tension is more prone to asymmetry effects. The basic characteristics of the J-Δa diagram for the three tests are as follows: in all three tests the blunting period lasts until $\Delta a \sim 0.08\,\mathrm{mm}$, and the values of J_c are 500, 2000, and 1700, $\mathrm{J/m^2}$ respectively.

Comparing Figure 1 to Figure 7, note that the initial part (AB) of the diagram corresponds to the formation of the plastic zone around the tip of the crack which causes a change in the crack length, see Figure 11. Then, the crack begins to extend and finally it

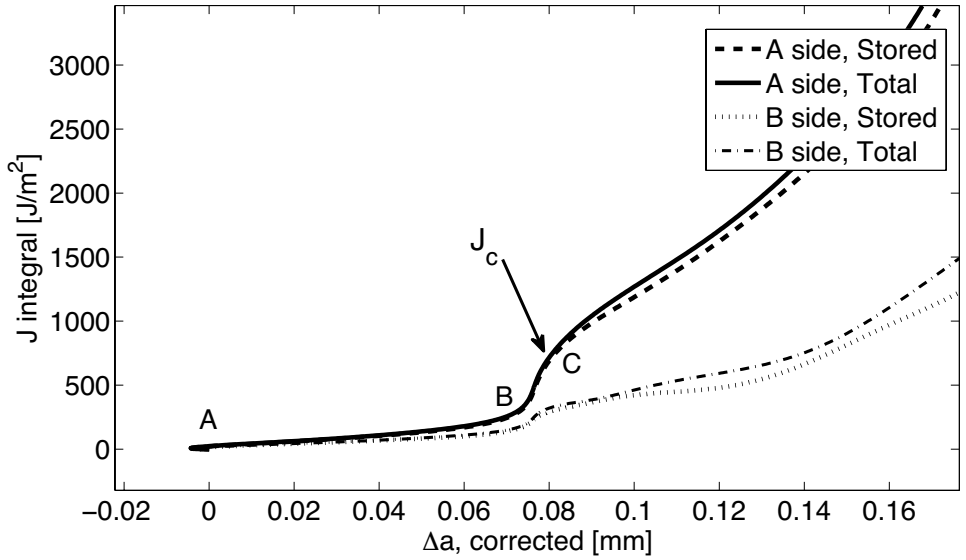

Figure 7: Variation of J-integral with crack size, for uniaxial test at 253 K and 1.33×10^{-4} s^{-1}.

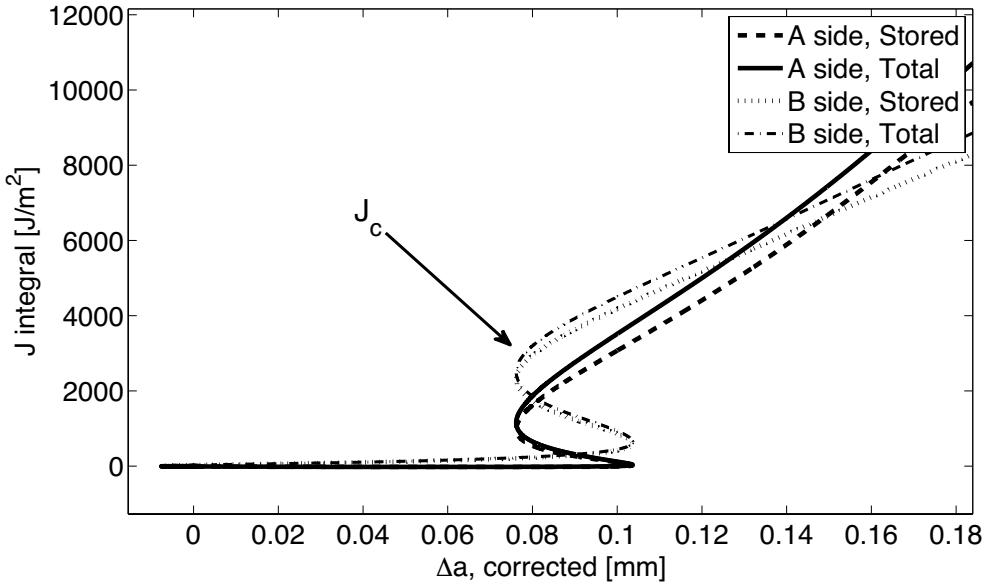

Figure 8: Variation of J-integral with crack size, for uniaxial test at 253 K and 1.33×10^{-5} s^{-1}.

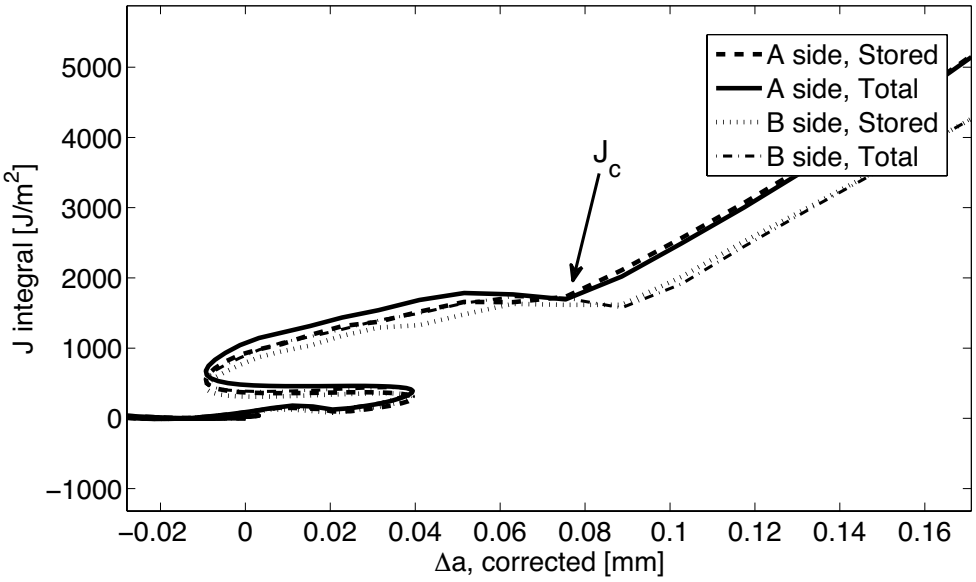

Figure 9: Variation of J-integral with crack size, for bubble test at 253 K.

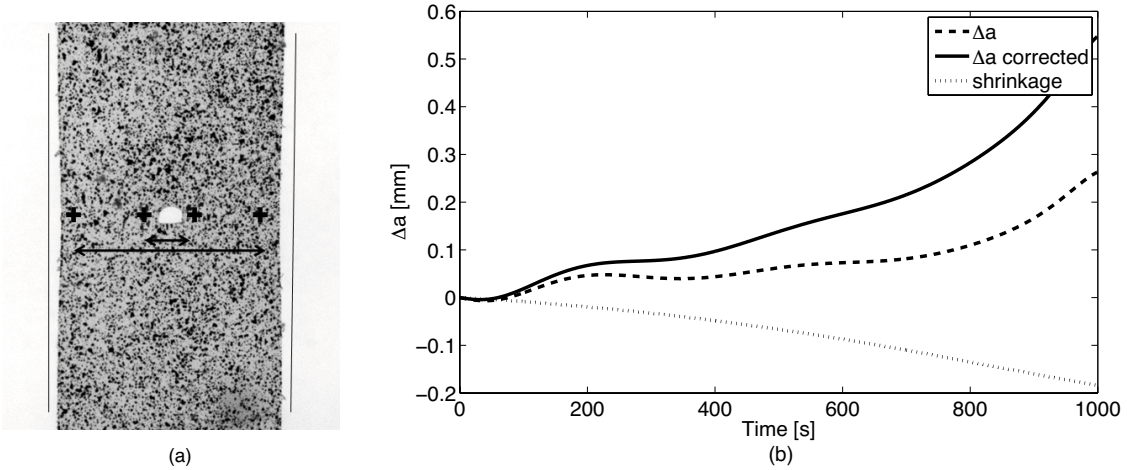

Figure 10: Effects of transverse deformation (a) reduction in overall width of sample and (b) change of crack size during uniaxial test at 253 K and 1.33×10^{-4} s^{-1}.

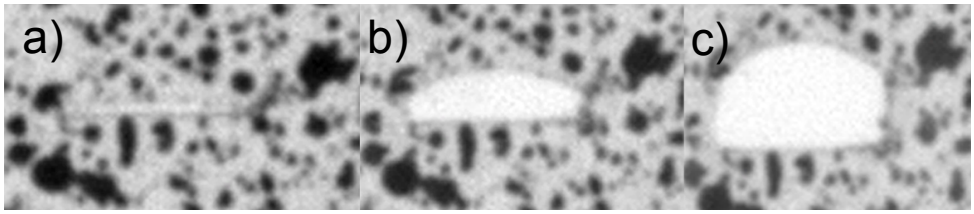

Figure 11: (a) initial crack shape, (b) blunted crack begins to propagate and (c) propagating crack, for uniaxial test at 253 K and 1.33×10^{-4} s^{-1}.

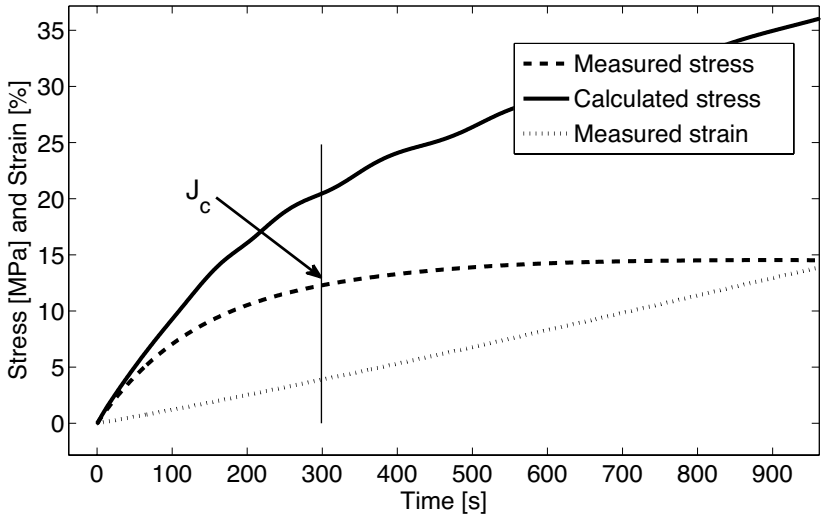

Figure 12: Comparison of average stresses in dogbone sample far from the crack (253 K, 1.33×10^{-4} s^{-1}).

propagates from C onwards. Figures 7 and 8 show a more complex variation before the critical value of J is reached.

Figure 12 shows a plot of the longitudinal average strain and the measured stress (obtained by dividing the stress by the initial cross-sectional area) during the full duration of a particular uniaxial test. A third plot shows the computed average stress during the same test, whose value was obtained from the longitudinal stress across a cross-section of the sample, derived from the strain field measured with DIC and converted to stress using the constitutive model. The time at which the crack began to propagate in this test is shown. It can be seen from these plots that the stress estimate is significantly higher than the measured stress, and it is about 30% too high when the critical crack amplitude is reached. Hence it can be concluded that our estimate of J_c for this test would also be higher than the actual value by a corresponding amount.

6 Discussion and Conclusion

The first question addressed in this study was the selection of a test sample configuration to study the failure behavior of LLDPE thin films. A comparison between the force-extension diagrams of pristine dogbone samples of StratoFilm 420 vs. samples with either pinholes or 2 mm wide transverse slits has produced comparable strength values. The third configuration has the advantage that the region of greatest interest in the sample is known from the beginning of the test, and hence high-resolution imaging of this region is possible, thus achieving greater accuracy in the measurement of the strain field in the region where failure occurs. For this reason, the 2 mm wide slit configuration was selected for further study.

Once this choice had been made, uniaxial tests on dogbone samples were carried out at two different strain rates, and a further test was carried out on a pressure-loaded circular diaphragm. Testing dogbone samples has the advantage that it is easier to set up and the overall strain rate can be easily controlled. Testing a pressurized diaphragm has the advantage that the stress distribution more clearly resembles the operation conditions of StratoFilm in a balloon structure.

Having calculated the variation of the J-integral on either side of initially 2 mm wide slits, in both test configurations we found that the critical increase in crack amplitude is ~ 0.08 mm and the critical value of the J-integral is in the range 500-2000 J/m^2 at a temperature of 253 K. We also found that the value of J_c increased by a factor of 4, from ~ 500 to ~ 2000 J/m^2 when the strain rate was increased by an order of magnitude, from 1.33×10^{-4} s^{-1} to 1.33×10^{-5} s^{-1}. Lastly, we found that the free volume constitutive model based on Rand[2] and Kwok[5] tends to over-predict the average stress in a dogbone sample, by around 30% at the strain of $\sim 4\%$ at which the critical value of J was reached.

Based on the results of the present study, a more extensive investigation of the J-integral around 2 mm wide slits in dogbone specimens of StratoFilm 420 will be required, including a range of temperateres and strain rates, in order to develop models for the energy dissipation near a propagating crack. Such models could be used to analyze the combinations of pressure and time that lead to failure in a structure made of StratoFilm 420. Also, a refinement of the large-strain constitutive model for StratoFilm 420 would be desirable.

ACKNOWLEGEMENTS: We thank Prof. W. Knauss for helpful comments and advice. DH research at the California Institute of Technology was supported by an Imre Koranyi Civi Engineering Fellowship from the Thomas Cholnoky Foundation. Financial support from the NASA Balloon Research Program is gratefully acknowledged.

REFERENCES

[1] Cathey H.M. and Pierce D.L. Development of the NASA Ultra-Long Duration Balloon. *NASA Science Technology Conference* (2007) NSTC2007, Paper C3P3.

[2] Rand, J.L., *An improved constitutive equation for SF420.* Winzen Engineering 2008.

[3] Rand, J.L., Wakefield, D., Studies of thin film nonlinear viscoelasticity for superpressure balloons. *Advances in Space Research*. (2010) **60**:45–56.

[4] Kwok, K., and Pellegrino, S., Large strain viscoelastic model for balloon film. *11th AIAA ATIO Conference* 20-22 September 2011, Virginia Beach, AIAA-2011–6939.

[5] Kwok, K., *Mechanics of Viscoelastic Thin-Walled Structures*. Caltech, PhD thesis 2012.

[6] Knauss, W., Time Dependent Fracture of Polymers. *Int. Series on the Strength and Fractures* (1989) 2683–2711.

[7] Brown, B., Lu, X., A fundamental theory for slow crack growth in Polyethylene. *Polymer* (1995) textbf36(3):543–548.

[8] Brinson, H.F., Brinson, L.C., *Polymer Engineering Science and Viscoelasticity*. Springer, 2008.

[9] Tielking, J.T., A fracture thoughness test for polymer film. *Polymer testing*. (1993) **12**:207–220.

[10] Coleman, B.D. and Noll, W., Foundations of linear viscoelasticity. *Reviews of Modern Physics*. (1961) **33**:239–249.

[11] Christensen, R.M., *Theory of Viscoelasticity: An Introduction*. Academic Press, Second Edition, 1982.

[12] Ferry, J.D., *Viscoelastic Properties of Polymers*. John Wiley and Sons, Third Edition, 1980.

[13] Flugge, W., *Viscoelasticity*. Springer-Verlag, 1975.

[14] Williams, M.L., Landel, R.F., and Ferry, J.D., The temperature dependence of relaxation mechanisms of amorphous polymers and other glass-forming liquids. *Journal of the American Chemical Society*. (1955) **77**:3701-3707.

[15] Knauss, W.G., Emri, I.J., Nonlinear viscoelasticity based on free volume consideration. *Computers and Structures*. (1981) **13**:123–128.

[16] Knauss, W.G., Emri, I.J., Volume change and the nonlinearly thermo-viscoelastic constitution of polymers. *Polymer Engineering and Science*. (1987) **27**:86–100.

[17] Young, L., *CTE curve fitting data*. NASA Balloon Program Office report, 2010.

[18] Naghdi, P.M., Murch, S.A., On the Mechanical Behavior of Viscoelastic/Plastic Solids. *Journal of Applied Mechanics*. (1963) 321–328.

[19] Crochet, M.J., Symmetric Deformations of Viscoelastic-Plastic Cylinders. *Journal of Applied Mechanics*. (1966) 327–334.

[20] Bruler, O.S., The energy balance of a viscoelastic material. *International Journal of Polymer Materialsn*. (1973) **2**:137–148.

[21] Bruler, O.S., The energy ballance of a viscoelastic material. *International Journal of Polymer Materials*. (1981) **21(3)**:145–150.

[22] Brinson, H.F., Matrix dominated time dependent failure prediction in polymer matrix composites. *Composite Structures*. (1999) **47**:445–456.

[23] Rice, J.R., Rosengren, G.F., Plane strain deformation near a crack tip in a power-law hardening material. *Journal of Mechanics, Physics and Solids*. (1968) **16**:1–12.

[24] Begley, J.A., Landes J.D., The J integral as a fracture criterion. *ASTM STM*. (1972) **515**:1–23.

[25] Sutton, M. A., Orteu, J. J., and Schreier, H. W., *Image correlation for shape, motion and deformation measurements: basic concepts, theory and applications*. Springer, 2009.

[26] Lai, J., Bakker, A., 3-d Schapery representation for nonlinear viscoelasticity and finite element implementation. *Computational Mechanics*. (1996) **18**:182–191.